RJC

RASĀYAN *J. Chem.*
Vol. 18 | No. 1 |600-606| January - March | 2025
ISSN: 0974-1496 | e-ISSN: 0976-0083 | CODEN: RJCABP
http://www.rasayanjournal.com
http://www.rasayanjournal.co.in

IMPACT OF SOLVENT VARIABILITY ON THE SYNTHESIS OF MnO_2/C COMPOSITE ELECTRODE FROM CORN COB-DERIVED ACTIVATED CARBON FOR ENHANCED SUPERCAPACITOR CAPACITANCE

Dyah Purwaningsih✉, A.K. Prodjosantoso, Siti Marwati and Dhaifina Vennyka Setiarini

Department of Chemistry Education, Universitas Negeri Yogyakarta, 55281, Indonesia
✉Corresponding author: dyah_purwaningsih@uny.ac.id

ABSTRACT

This study investigates the impact of solvents (methanol, ethanol, 2-propanol, ethylene glycol, and polyethylene glycol) on the synthesis of MnO_2/C composites derived from activated carbon from corn cobs, focusing on crystalline structure, surface area, and morphology. Additionally, it evaluates the specific capacitance of MnO_2/C composites for supercapacitor applications. MnO_2/C was synthesized via a solvothermal method, with solvent selection being key to optimizing capacitance. The process involved two stages: activated carbon preparation and solvothermal treatment. Various characterization techniques (SEM, TEM, SAA, XRD) and capacitance testing were employed to assess the properties and performance of the composites. The study found that MnO_2/C synthesized with ethanol as the solvent achieved the highest specific capacitance of 47 mF/g, outperforming other solvents. X-ray diffraction (XRD) analysis revealed MnO_2 crystals with a crystallinity size of 20.55 nm in the α-MnO_2phase, making the composite highly suitable for supercapacitors. Surface area analysis (SAA) showed the highest surface area for the ethanol-based composite (239.608 m^2/g), followed by ethylene glycol (238.816 m^2/g), and methanol (196.62 m^2/g). SEM-EDX confirmed the good deposition of MnO onto the carbon, with 54.66% MnO and 40.90% carbon. TEM revealed a polycrystalline structure in ethanol-derived MnO_2/C, enhancing surface area. These results highlight how ethanol's solubility, polarity, and molecular dimensions optimize the solvothermal process, leading to uniformly distributed MnO_2 deposition.

Keywords: Activated Carbon, MnO_2, Supercapacitors, Solvent, Capacitance Value.

RASĀYAN *J. Chem.*, Vol. 18, No.1, 2025

INTRODUCTION

The demand for electrical power in Indonesia is rising, driven by growth in the industry, transportation, and residential sectors.[1] In response, energy storage technologies like supercapacitors, known for their high-power density (103–104 W/kg), long cycle life (>100,000 cycles), rapid charging, and eco-friendly nature, are gaining attention. Biomass waste, rich in activated carbon, offers a promising material for supercapacitors due to its high surface area, stability, and excellent conductivity.[2] Various biomass sources, such as corn cobs, bagasse, coconut shells, and rice husks, are valuable raw materials for activated carbon production. Activated carbons from corn cobs, specifically, exhibit a significant surface area, moderate mesoporosity, and a pore structure combining mesopores and micropores.[3] Enhancing this carbon with additional materials can significantly improve capacitance. Introducing MnO_2 into supercapacitors boosts energy density, as MnO_2 possesses pseudocapacitive properties and a large surface area.[4] Its pseudocapacitance synergizes with activated carbon's dual capacitance, increasing the overall capacitance. Several synthesis methods, including hydrothermal, solvothermal, electrospinning, and coprecipitation, have been used to create MnO_2/activated carbon composites.[5] For instance, hydrothermally synthesized α-MnO_2/C composites have achieved a capacitance of 977.4 F/g and a cycle life of 3000 cycles, demonstrating their potential as supercapacitor electrode materials.[6]

In this study, MnO_2/C will be synthesized using the solvothermal method, chosen for its ability to control particle size, morphology, and purity.[7] This method is influenced by factors such as reagent nature, solvent choice, temperature, and pressure. The study will optimize solvent selection for MnO_2/C synthesis, using solvents like methanol, ethanol, 2-propanol, ethylene glycol, and polyethylene glycol.

EXPERIMENTAL

The research material utilized was corn cob waste. Chemicals of Pro Analyst Merck quality such as KOH, $KMnO_4$, $MnSO_4$, Methanol, Ethanol, 2-Propanol, Ethylene Glycol (EG), Polyethylene Glycol (PEG), PVA, and Na_2SO_4 were employed, alongside 96% ethanol and distilled water.

http://doi.org/10.31788/RJC.2025.1819160

The equipment included an E-scientific muffle furnace, porcelain pestle and mortar, mesh 100, Whatman filter paper, eDAQ potentiostat, X-ray diffraction (XRD), scanning electron microscopy (SEM) with energy dispersive X-ray spectroscopy (EDX), transmission electron microscopy (TEM), surface area analyzer (SAA), and a sonicator. Corn cob-activated carbon was prepared by slicing the cobs into 3 cm fragments, cleaning, and sun-drying them. The dried cobs were combusted in a furnace at 750°C for 1.5 hours and then pulverized with a mortar and pestle. The resulting carbon was sieved through a 100-mesh screen. For activation, KOH was added to the carbon in a 3:1 ratio (KOH: carbon) and stirred at room temperature for 24 hours, followed by drying in an oven at 80°C for 24 hours. After activation, the dried carbon was rinsed with distilled water and ethanol until neutral pH was achieved, then dried again at 80°C for 24 hours. The dried activated carbon was then analyzed using XRD and SEM. For MnO_2/C synthesis, 0.4 g of activated carbon was dispersed in 40 ml of ethanol and sonicated for 20 minutes to ensure homogeneity. Separately, 0.2 g of $MnSO_4$ and 0.2 g of $KMnO_4$ were dissolved in 10 ml of distilled water, stirred for 30 minutes, and added to the activated carbon solution. The mixture was sonicated for 10 minutes and transferred to a Teflon-lined stainless-steel autoclave, which was then placed in an oven at 90°C for 24 hours. After cooling, the solids were washed with distilled water and ethanol until neutral pH, and the wet composite was dried overnight at 50°C. This procedure was repeated with four other solvent variations, followed by XRD, SAA tests, and capacitance analyses.

RESULTS AND DISCUSSION

XRD Analysis

The comparison of diffraction patterns between activated carbon and MnO_2/C (methanol, ethanol, 2-propanol, ethylene glycol, and polyethylene glycol) is shown in Fig.-1. Activated carbon exhibits a broad peak in its XRD pattern, indicating an amorphous phase. The pattern closely resembles ICDD database No. 41-1487, with peaks at 2θ positions of 24.91° and 44.25°, corresponding to the 002 and 100 lattice planes of Graphite 2-H. The XRD pattern of MnO_2/C with various solvents reveals two distinct phases: MnO_2 (ICDD No. 44-0141) and carbon (Graphite-2H, ICDD No. 41-1487). Sharp peaks indicate the formation of crystalline phases. The carbon phase shows peaks at 2θ positions around 24-26°, 43-45°, and 54-55°, corresponding to the (002), (101), and (004) lattice planes in the hexagonal crystal system. Peaks for the MnO_2 phase appear at 2θ values near 28-29°, 35-38°, 40-42°, 47-49°, and 63-66°, matching the (310), (211), (420), (510), and (002) lattice planes.

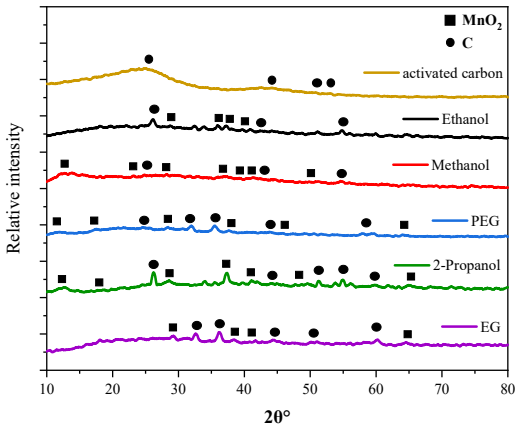

Fig.-1: Contrast of diffraction Patterns Between Activated Carbon and MnO_2/C in Ethanol, Methanol, PEG, 2-propanol, and Ethylene Glycol

The carbon phase in MnO_2/C PEG and MnO_2/C EG displays a cubic crystal structure at 2θ values around 31-33° and 35-36°, consistent with ICDD No. 18-0311. This cubic structure results from hydrogen bonding between hydroxyl groups (-OH) in the solvent and the MnO_2 surface. The tetragonal phase of MnO_2 is suggested to improve supercapacitor performance by increasing ion conductivity, according to previous research.[8] The crystallite size can be determined by analyzing each crystalline peak using the Debye-Scherer equation of $D = \frac{K.\lambda}{\beta.\ cos\theta}$, where D is crystallite size, K is the Scherer constant, λ is the Cu Kα wavelength, β is the full width at half maximum (FWHM), and $cos\theta$ is the peak position angle. The calculated crystallite sizes are presented in Table-1.

Table-1: Comparison of Crystalline Dimensions with Variations in Solvent Composition

No	Sample	Solvent	Size (nm)
1	MnO_2/C	Ethanol	20.55
2	MnO_2/C	Methanol	53.32
3	MnO_2/C	Polyethylene Glycol	86.68
4	MnO_2/C	2-propanol	60.35
5	MnO_2/C	Ethylene Glycol	28.04

Crystallite size analysis revealed that solvent polarity affects crystal size, following this hierarchy: ethanol < ethylene glycol < methanol < 2-propanol < polyethylene glycol. Solvents with lower polarity, like 2-propanol, resulted in larger crystals, while higher polarity solvents like ethanol, methanol, and ethylene glycol yielded smaller crystals, aligning with previous research.[9] However, solvent molecular size also plays a crucial role, with larger molecules promoting larger crystals due to steric hindrance.[10] Ethanol's smaller molecular size and lower solubility compared to methanol resulted in smaller crystals, enhancing conductivity and specific capacitance.[11]

SEM-EDX Analysis of Activated Carbon

The surface morphology of corn cob-activated carbon shows layered particles that aggregate to form hollow spaces. At 5000× and 10000× magnification, round pores are visible within these spaces. At 25000×, the layer surfaces are coated with irregularly dispersed tiny particles.

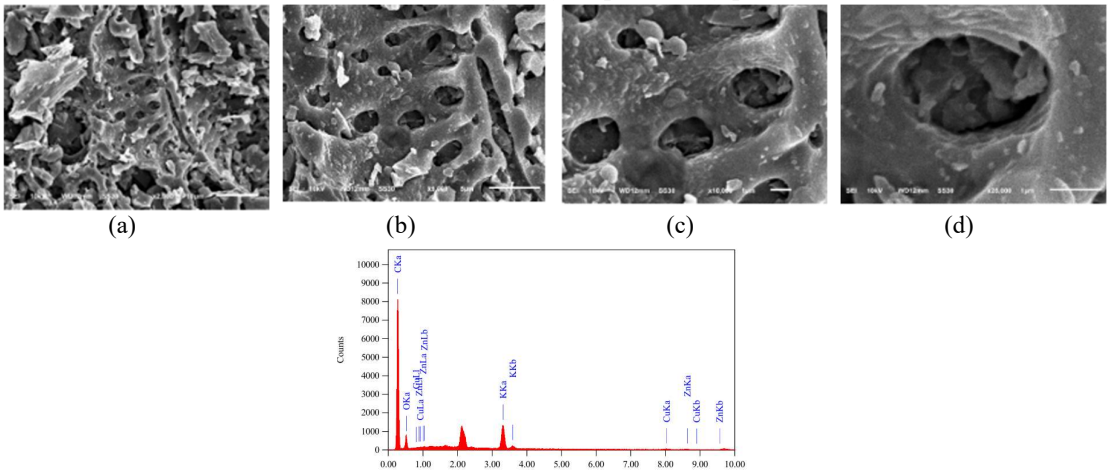

Fig.-2: SEM Analysis Findings on Activated Carbon Illustrating SEM Morphology at Various Magnifications: 500× (a), 2000× (b), 10000× (c), and 25000× (d), alongside EDX Results (e)

The EDX analysis confirms that the small particles are in the carbon oxide form. At a magnification of 2000× (Fig. 2b), the main elements in corn cob-activated carbon are carbon, oxygen, and potassium, with compositions of 68.62%, 18.75%, and 9.15%, respectively. Additionally, trace amounts of copper and zinc, natural minerals in corn cobs, were detected at 2.07%, and 1.42%, respectively.

Analysis of SAA Test Results with BET and BJH Methods

Surface area analysis of corn cob-derived activated carbon, conducted using SAA, showed a surface area of 240.712 m^2/g and a pore volume of 0.14206 cc/g. This large area meets the requirements for its application as a pseudocapacitors electrode. The SEM images further reveal that the layered particle structure creates voids, which likely serve as sites for pore formation.

According to IUPAC, the resulting curve is a combination of Type I and Type II, typical of mesoporous materials. The increase at low relative pressure (P/P0 < 0.2) indicates the formation of micropores, while the sharp rise at high relative pressure (P/P0 > 0.8) signifies the presence of macropores.[12]

Table-2 presents the specific surface area (SBET) of MnO_2/C samples synthesized with different solvents, ranked as methanol > ethylene glycol > ethanol > 2-propanol > polyethylene glycol. Methanol-based MnO_2/C has the highest surface area, which aligns with pore volume findings. An increase in pore volume typically corresponds to a higher surface area, as more pores provide additional surface area.[13] Higher solvent polarity enhances pore formation; methanol's ability to form hydrogen bonds with precursors stabilizes hydroxyl groups, resulting in smaller particles and increased surface area.[14]

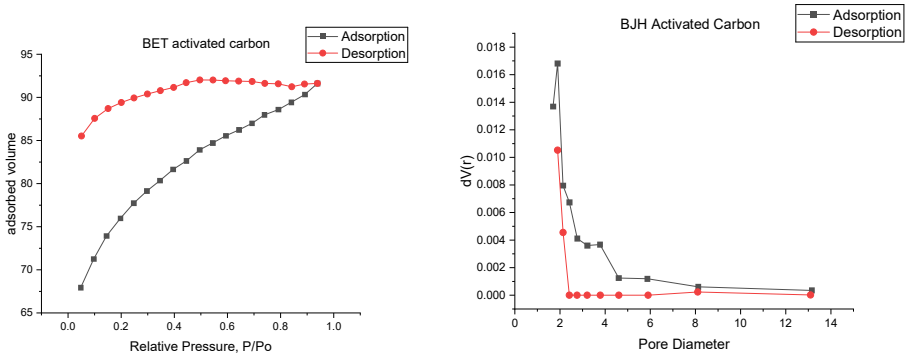

Fig.-3: Adsorption-Desorption Isotherm Curve and BJH Plot of N_2 Activated Carbon

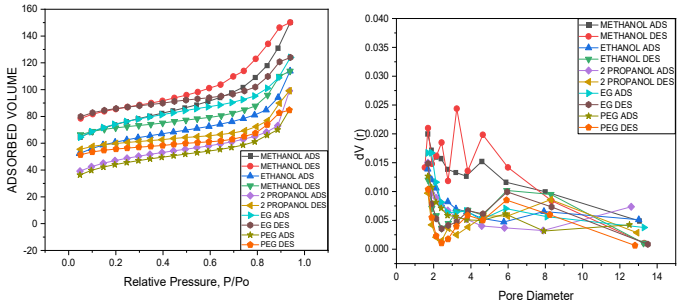

Fig.-4: N_2 Adsorption-Desorption Isotherm Curve of MnO_2/C Composite with Methanol, Ethanol, 2-Propanol, Ethylene Glycol, and Polyethylene Glycol Solvents

Table-2: SAA Analysis Results

Solvent Variation	Surface Area (m^2 /g)	Pore Volume (cc/g)	Pore Size (nm)
Methanol	239.61	0.233	1.944
Ethanol	196.62	0.176	1.796
2-Propanol	154.63	0.154	1.988
Ethylene Glycol	238.82	0.192	1.611
Polyethylene Glycol	144.93	0.131	1.813

In contrast, polyethylene glycol's long chains reduce surface area due to aggregation. Ethanol also reduces particle size and improves surface area by preventing agglomeration.[15] Pore size analysis reveals that all samples fall within the micropore range ($r \leq 2$ nm).[16] A balanced presence of micropores and mesopores optimizes capacitance and power density in aqueous electrolytes.[17]

Capacitance Test Results

Figure-5(a) shows a narrow CV curve for methanol, with a capacitance of 11.19 mF/g, indicating limited interaction between the electrode material and ions, likely due to the small size of methanol molecules. As a result, methanol yields lower capacitance than ethanol. The broader CV curve of ethanol, with a substantial loop, reflects better ion interaction, enhanced conductivity, and electrode durability, resulting in a high capacitance of 47 mF/g, making it the optimal solvent in this study. The CV curve of 2-propanol also shows good performance, with a capacitance of 45.67 mF/g. In contrast, ethylene glycol (5.54 mF/g) and polyethylene glycol (8.79 mF/g) display lower capacitance, likely due to their higher viscosity, which hinders ion mobility and charge storage efficiency.

Calculation of Capacitance Value

Voltammograms of composite electrodes exhibit peaks corresponding to oxidation and reduction reactions at the electrode-electrolyte interface, indicating the pseudocapacitive properties of MnO_2.[18] The specific capacitance (Cp) is calculated by determining the area under the curve using OriginPro 2023 software and applying the formula $p = \frac{A}{2mk(V1-V2)}$, where A is the area, m is the electrode mass (g), k is the scan rate (mV/s), and (V1-V2) is the potential window.

(a) (b)

Fig.-5: Comparison of CV Curves of Various Solvents (a); the Capacitance Value Resulting from the Utilization of Activated Carbon and Various Solvents (b)

Figure-5(b) compares the capacitance values of activated carbon and MnO_2 synthesized with various solvents including methanol, ethanol, 2-propanol, ethylene glycol, and polyethylene glycol. The addition of MnO_2 enhances capacitance across all composites. Ethanol-based composites exhibit the highest capacitance (47 mF/g), followed by 2-propanol (45.67 mF/g). In contrast, composites with methanol, ethylene glycol, and polyethylene glycol show lower capacitance of 11, 5.549, and 8.797 mF/g, respectively. Ethanol effectively promotes the formation of a stable MnO_2/C structure, improving energy storage capacity compared to other solvents.

Comparison of CV Curve and Capacitance Value of Solvent Variation

Fig.-5(a) presents the rectangular CV curve of ethanol, showing excellent capacitive behavior.[19] An optimal electrolyte should have a broad potential window, low resistance, low viscosity, non-flammability, high electrochemical stability, and eco-friendliness.[20] Ethanol and 2-propanol, with relatively low viscosities, facilitate solvent penetration into activated carbon pores, aiding MnO_2 structure formation. Lower viscosity enhances solvent flow during the solvothermal process, ensuring well-organized MnO_2 distribution. In contrast, the higher viscosity of ethylene glycol hinders solvent diffusion, leading to irregular MnO_2 formation and reduced capacitance. Ethanol and 2-propanol, due to their simple chemical structure and hydroxyl groups (-OH), interact more effectively with MnO_2 precursors and activated carbon. These hydroxyl groups improve precursor solubility and MnO_2 adhesion to the carbon surface, enhancing distribution and supercapacitor performance. Gromadskye (2015) found that highly polar solvents can restrict pore space, hindering ion transfer from the electrolyte to the pores.[21] As a result, methanol, with its higher polarity, shows lower capacitance compared to ethanol and 2-propanol. Ethylene glycol, with two -OH groups, has weaker interactions with the precursors, while polyethylene glycol, with more -OH groups and a larger molecular weight, leads to uneven MnO_2 distribution, reducing the effective surface area for electrostatic reactions. According to IEC/EN 62391-1: 2006, the ethanol-based composite, with a capacitance of 47 mF/g (0.0471 F/g), qualifies as a Class I supercapacitor. Class I supercapacitors are suitable for energy storage applications with a frequency range of 0.047 to 0.6 Farad at 0.105 Hz and a 30-minute charging time, typically used for memory backup.

SEM-EDX Analysis of Ethanol

MnO_2/C composites synthesized with various solvents showed ethanol as the optimal choice, determined by XRD, surface area measurements, and highest capacitance. SEM-EDX analysis of the ethanol-derived composite's surface morphology is shown in Fig.-6.

At a magnification of 2000×, SEM images show stratified particles forming cavities that enhance energy storage by promoting ion interaction. At 25000× magnification, small particles are observed in a non-uniform distribution across the surface, likely manganese dioxide (MnO_2) that plays a key role in the pseudocapacitor's redox mechanism, improving capacitance. EDX analysis (Fig.-6e) reveals the elemental composition of MnO_2/C, with atomic ratios of 58.66% carbon (C), 24.35% oxygen (O), and 13.41% manganese (Mn). Trace elements include fluorine (F), magnesium (Mg), potassium (K), and copper (Cu) at 3.28%, 0.02%, 0.24%, and 0.04%, respectively. A quantitative EDX assessment shows mass percentages of 40.90% carbon, 54.66% manganese oxide (MnO), 3.56% fluorine, 0.05% magnesium oxide (MgO), 0.66% potassium oxide (K_2O), and 0.17% copper oxide (CuO). The uniform distribution of MnO_2 on activated carbon is reflected in the minimal variation between carbon and manganese oxide percentages. This consistency highlights how ethanol's solubility, polarity, and molecular dimensions optimize the solvothermal process, promoting more uniform MnO_2 deposition on activated carbon.

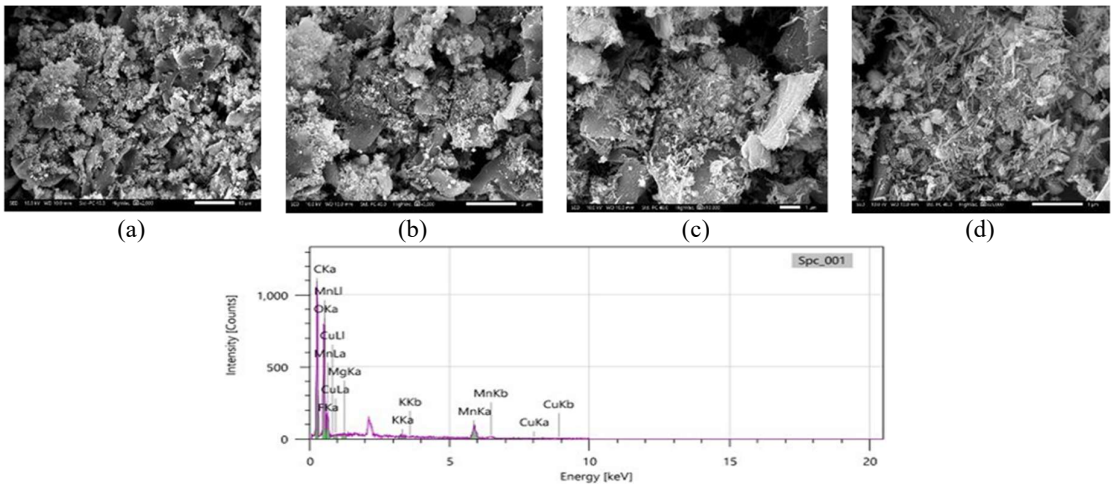

Fig.-6: SEM Analysis Results on Activated Carbon Showcasing SEM Morphology at a Magnification of 500× (a), 2000× (b), 10000× (c), and 25000× (d), along with EDX (e)

TEM SAED Analysis of MnO_2/C in Ethanol

The polycrystalline structure, indicated by multiple focal points in the SAED diffraction pattern, suggests the presence of randomly oriented crystallites within the electrode material. This enhances the active surface area, promoting more charge storage sites and ion diffusion, crucial for increasing supercapacitor capacitance. The complex diffraction pattern also improves the interaction between the electrode material and electrolyte ions, leading to better specific capacitance and cycling performance in supercapacitors.

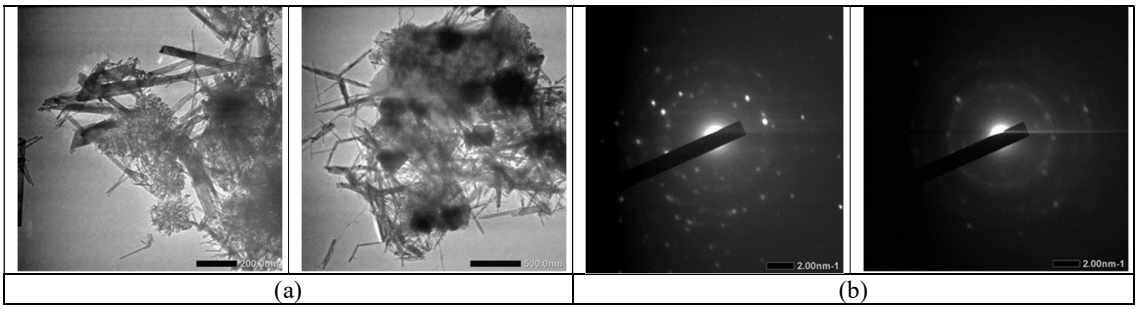

Fig.-7: TEM (a) SAED (b) Analysis Results of MnO_2/C in Ethanol

CONCLUSION

XRD analysis revealed that ethanol solvent produced MnO_2 crystals with a size of 20.55 nm in the α-MnO_2 phase, ideal for supercapacitors. The ethanol composite showed a surface area of 196.62 m^2/g with microporous structures. SEM-EDX analysis indicated 54.66% MnO and 40.90% carbon in the MnO_2/C composite. TEM confirmed a polycrystalline structure and increased surface area. Ethanol's properties enhanced the solvothermal process, ensuring uniform MnO_2 deposition on activated carbon. Cyclic voltammetry testing showed the highest specific capacitance of 47 mF/g, suitable for memory backup. The superior capacitance with ethanol is due to its reduced crystalline size, diverse pore sizes, and optimized pore structure, improving ion diffusion and charge storage.

ACKNOWLEDGMENTS

The study was supported by DRTPM through the *Penelitian Fundamental Reguler* (PFR) Program. The authors also acknowledge Hari Muryanto for language assistance and final draft improvements.

CONFLICT OF INTEREST

The authors declare that there is no conflict of interest

AUTHOR CONTRIBUTIONS

All the authors contributed significantly to this manuscript, participated in reviewing/editing and approved the final draft for publication. The research profile of the authors can be verified from their ORCID ids, given below:

Dyah Purwaningsih https://orcid.org/0000-0003-2546-0954
Anti Kolonial Prodjosantoso https://orcid.org/0000-0001-7603-5857
Siti Marwati https://orcid.org/0000-0001-6498-9565
Dhaifina Vennyka Setiarini https://orcid.org/0009-0005-9550-0001

REFERENCES

1. P.Y. So, *E-Journal Graduate Unpar*, **1**, 1(2014).
2. A. Awitdrus, Z. Hanifa, A. Agustino, E. Taer, and R. Farma, *Indonesian Journal of Industrial Research*, **12**, 15(2022), https://doi.org/10.24960/jli.v12i1.7206.15-20
3. M. Karnan, K. Subramani, P.K. Srividhya, and M. Sathish, *Electrochimica Acta*, **228**, 586(2017), https://doi.org/10.1016/j.electacta.2017.01.095
4. N. Nursiti, E.R. Wibowo, A.W. Safitri, S. Supriyono, and R. Oktavian, *Jurnal Chemurgy*, **2**, 6(2018), https://doi.org/10.30872/cmg.v2i1.1631
5. J. Jablonskiene, D. Simkunaite, J. Vaiciuniene, G. Stalnionis, A. Drabavicius, V. Jasulaitiene, V. Pakstas, L. Tamasauskaite-Tamasiunaite, and E. Norkus, *Crystals*, **11(7)**, 784(2021), https://doi.org/10.3390/cryst11070784
6. Y. Yang, H. Niu, F. Qin, Z. Guo, J. Wang, G. Ni, P. Zuo, S. Qu, and W. Shen, *Electrochimica Acta*, **354**, 136667(2020), https://doi.org/10.1016/j.electacta.2020.136667
7. G. Demazeau and A. Largeteau, *Zeitschrift fur Anorganische und Allgemeine Chemie*, **641**, 159(2015), https://doi.org/10.1002/zaac.201400515
8. K. Belova, A. Egorova, S. Pachina, and I. Animitsa, *Applied Sciences*, **12**, 1181(2022), https://doi.org/10.3390/app12031181
9. M. Bilal, B. Ambreen, J. Ali, and I. Shahid, *Iranian Journal of Chemistry and Chemical Engineering*, **38**, 261(2019), https://doi.org/10.30492/ijcce.2019.31718
10. Y. Wang and Z. Liang, *CrystEngComm*, **19**, 3198(2017), https://doi.org/10.1039/C7CE00474E
11. Parashtekar, L. Bourgeois, and S.S.V. Tatiparti, *Journal RSC Advances,* **12**, 8333(2022), https://doi.org/10.1039/D1RA09000C
12. K. Zheng, Y. Li, M. Zhu, X. Yu, M. Zhang, L. Shi, and J. Cheng, *Journal of Power Sources*, **366**, 270(2017), https://doi.org/10.1016/j.jpowsour.2017.09.034
13. Prayitno, D, *Metrik Serial Teknologi dan Sains*, **5(2)**, 111(2024), https://publikasi.kocenin.com/index.php/teksi/article/download/583/478/1006
14. L.L. Pote, A. Nadut, and G. Latumakulita, *Jurnal Sains dan Edukasi Sains*, **7**, 118(2024), https://doi.org/10.24246/juses.v7i2p118-127
15. P.P. Upare, Y.K. Hwang, J.C. Kim, J.H. Lee, S.K. Kwak, and D.W. Hwang, *ChemSusChem*, **13**, 5050(2020), https://doi.org/10.1002/cssc.202001323
16. K.K. Yadav, R. Wadhwa, N. Khan, and M. Jha, *Current Research in Green and Sustainable Chemistry*, **4**, 100075 (2021), https://doi.org/10.1016/j.crgsc.2021.100075
17. E. Taer, M. Melisa, A. Agustino, R. Taslim, W.S. Mustika, and A. Apriwandi, *Energy Sources, Part A: Recovery, Utilization and Environmental Effects*, pp. 1–12(2021), https://doi.org/10.1080/15567036.2021.1950871
18. X. Wang, S. Chen, D. Li, S. Sun, Z. Peng, S. Komarneni, and D. Yang, *ACS Sustainable Chemistry and Engineering*, **6**, 633(2018), https://doi.org/10.1021/acssuschemeng.7b02960
19. X. Zhao, Y. Hou, Y. Wang, L. Yang, L. Zhu, R. Cao, and Z. Sha, *Journal RSC Advances*, **7**, 40286(2017), https://doi.org/10.1039/c7ra06369e
20. P. Galek, A. Slesinski, K. Fic, and J. Menzel, *Journal of Materials Chemistry A*, **9**, 8644(2021), https://doi.org/10.1039/d0ta11230e
21. D.G. Gromadskye, J.H. Chae, S.A. Norman, and G.Z. Chen, *Applied Energy*, **159**, 39(2015), https://doi.org/10.1016/j.apenergy.2015.08.108

[RJC-9160/2024]